Structural basis of jasmonate-amido synthetase FIN219 in complex with glutathione S-transferase FIP1 during the JA signal regulation

Chun-Yen Chen[a], Sih-Syun Ho[a], Tzu-Yen Kuo[a], Hsu-Liang Hsieh[a], and Yi-Sheng Cheng[a,b,c,1]

[a]Institute of Plant Biology, National Taiwan University, Taipei 10617, Taiwan; [b]Department of Life Science, National Taiwan University, Taipei 10617, Taiwan; and [c]Genome and Systems Biology Degree Program, National Taiwan University, Taipei 10617, Taiwan

Edited by Joseph P. Noel, Howard Hughes Medical Institute, La Jolla, CA, and accepted by Editorial Board Member Joseph R. Ecker January 17, 2017 (received for review June 21, 2016)

Far-red (FR) light-coupled jasmonate (JA) signaling is necessary for plant defense and development. FR insensitive 219 (FIN219) is a member of the Gretchen Hagen 3 (GH3) family of proteins in *Arabidopsis* and belongs to the adenylate-forming family of enzymes. It directly controls biosynthesis of jasmonoyl-isoleucine in JA-mediated defense responses and interacts with FIN219-interacting protein 1 (FIP1) under FR light conditions. FIN219 and FIP1 are involved in FR light signaling and are regulators of the interplay between light and JA signaling. However, how their interactions affect plant physiological functions remains unclear. Here, we demonstrate the crystal structures of FIN219–FIP1 while binding with substrates at atomic resolution. Our results show an unexpected FIN219 conformation and demonstrate various differences between this protein and other members of the GH3 family. We show that the rotated C-terminal domain of FIN219 alters ATP binding and the core structure of the active site. We further demonstrate that this unique FIN219–FIP1 structure is crucial for increasing FIN219 activity and determines the priority of substrate binding. We suggest that the increased FIN219 activity resulting from the complex form, a conformation for domain switching, allows FIN219 to switch to its high-affinity mode and thereby enhances JA signaling under continuous FR light conditions.

jasmonate response | far-red light | signaling cross-talk | adenylation enzyme | phytohormone

Far-red (FR) insensitive 219 (FIN219) (1), also known as jasmonate (JA) resistant 1 (JAR1; AtGH3.11) (2), is a member of the auxin-regulated Gretchen Hagen 3 (GH3) family of proteins (3). The GH3 family in *Arabidopsis* is composed of 19 distinct proteins and is also conserved in plants such as rice (4–6), tomato (7, 8), and maize (9), with 13, 15, and 13 members, respectively. Phylogenetically, the GH3 family is classified as part of the adenylate-forming enzyme superfamily, which contains proteins such as firefly luciferase-like enzymes (10). This diverse group of enzymes catalyzes the addition of AMP to carboxyl groups on a wide variety of substrates and typically contains three conserved motifs that form a binding pocket for ATP and AMP substrate intermediates (11). GH3 proteins regulate the activity of plant hormones through amino acid conjugation and have a substantial effect on plant metabolism and physiology (12). For example, FIN219 catalyzes the conjugation of isoleucine (Ile) to JA, forming jasmonoyl-isoleucine (JA-Ile). This reaction results in the degradation of the transcriptional repressor JA-ZIM (zinc-finger protein expressed in inflorescence meristem) domain (JAZ) proteins and the subsequent activation of downstream transcriptional responses (13).

FIN219 has been identified in suppressor screenings using a temperature sensitive *constitutive photomorphogenic 1* (*cop1*) mutant line. It is involved in FR light-mediated inhibition of hypocotyl elongation and regulates light inactivation of COP1 activity (1). Furthermore, FIN219 acts as a positive regulator of FR light signaling by directly interacting with the COP1 protein and suppressing its activity in the dark (14). Overexpression of FIN219 causes a FR-specific hyperphotomorphogenic response. During JA signaling, FIN219 catalyzes the conjugations between JA and various amino acids, such as leucine (JA-Leu), valine (JA-Val), or methionine (JA-Met) (15). The *fin219* mutants also have a reduced JA-Ile production and JA response (16). JA is an oxylipin derived from α-linolenic acid in plastid membranes that respond to biotic and abiotic stresses (17–24). It is also synthesized during flowering, during seed development, and in response to wounding (20, 22). Recent research has confirmed that JA regulates phytochrome A (phyA)-perceived FR light signaling (25). For example, the defective JA receptor *coronatine insensitive 1* (*coi1*), *phyA*, *jar1/fin219*, and *allene oxide synthase* (*aos*) mutants all have significantly longer hypocotyls under FR light in comparison to the wild-type plants (26). In addition, the FIN219 protein level is positively regulated by phyA under FR light in a fluence-dependent manner (14). To understand the connection between plant defense and light signals, it is necessary to identify the role of FIN219 and its interacting partners by clarifying the mechanism of molecular interplay between JA response and phyA-mediated FR light signaling.

FIN219-interacting protein 1 (FIP1), whose gene encodes the GST (AtGSTU20), is a member of the GST tau family, which is composed of 55 members in *Arabidopsis*. This family is involved in diverse functions, including detoxification and reduction of oxidative stress (27–29). FIP1 has a GST activity of specific affinity to glutathione (GSH) and 1-chloro-2,4-dinitrobenzene

Significance

Far-red (FR) insensitive 219 (FIN219) is the main jasmonate (JA)-amido synthetase that activates the systemic synthesis of bioactive JAs in *Arabidopsis*. FIN219 is involved in FR light signaling and interacts with another signaling component, FIN219-interacting protein 1 (FIP1). To extend our understanding of the regulatory mechanism between FR light signaling and the JA response, we determine the crystal structures of the FIN219–FIP1 complex with substrates and show that interaction with FIP1 triggers enhanced activity of FIN219. FIN219 conformational changes driven by FIP1 are observed in the C-terminal domain and show a relatively occluded form of the active site. By measuring the FIN219–FIP1 interaction and adenylation function, this study reveals that FIP1 may regulate FIN219 activity and further alters the level of JA signaling.

Author contributions: H.-L.H. and Y.-S.C. designed research; C.-Y.C., S.-S.H., and T.-Y.K. performed research; C.-Y.C., S.-S.H., and T.-Y.K. analyzed data; and C.-Y.C. and Y.-S.C. wrote the paper.

The authors declare no conflict of interest.

This article is a PNAS Direct Submission. J.P.N. is a Guest Editor invited by the Editorial Board.

Freely available online through the PNAS open access option.

Data deposition: The atomic coordinates and structure factors have been deposited in the Protein Data Bank, www.pdb.org (PDB ID codes 5ECH, 5ECI, 5ECK, 5ECL, 5ECM, 5ECN, 5ECO, 5ECP, 5ECQ, 5ECR, 5GZZ, and 5ECS).

[1]To whom correspondence should be addressed. Email: chengys@ntu.edu.tw.

This article contains supporting information online at www.pnas.org/lookup/suppl/doi:10.1073/pnas.1609980114/-/DCSupplemental.

(CDNB) substrates (30). Previous studies indicated that FIP1 interacts with FIN219 and is involved in the regulation of FR light signaling (30). Knockdown or knockout transgenic seedlings have a hyposensitive phenotype under continuous FR light and delay flowering when days are long (30). In *Arabidopsis*, the tau-class genes of GSTs may be activated if treated with phytohormone, herbicide, or hydrogen peroxide, or if inoculated with plant pathogens (31). In particular, the expression of tau GSTs that were upregulated by methyl-JA treatment was obviously higher than when treated with ethylene and salicylic acid (31). However, microarray assays have revealed a comparatively low transcriptional level of FIP1 in the whole *Arabidopsis* GST tau family (32). These studies imply that some regulatory mechanisms may exist to mediate between FIP1 and JA signaling. To date, GST members have been infrequently associated with light signaling at the molecular level, but a previous report suggested that FIP1 might interact with FIN219 under FR light to regulate seedling photomorphogenesis (30). Therefore, the FIP1 protein is thought to provide a direct link between light signaling and JA response.

Recent studies of the FIN219–JA-Ile complex structure demonstrate that its structural features are the structural features of adenylate-forming enzymes (33). They suggest that FIN219 is composed of a dynamic C-terminal domain, a larger active site in the N-terminal domain, and a flexible hinge linker controlling the C-terminal domain orientation for substrate binding (33–35). However, how FIN219 interacts with FIP1 and the molecular mechanism of FIN219–FIP1 during JA response remains unknown. To gain further insight into these mechanisms, we examined the crystal structures of the FIN219–FIP1 complex with substrates and the FIP1–GSH complex, as well as performing biophysical and biochemical analysis to illustrate the cooperative function of FIP1 for FIN219 adenylation activity.

Results

Crystal Structure of the FIN219–FIP1 Complex. A previous study identified the closed-form (AMP- and acyl acid-bound) and open-form (ATP-bound) GH3 protein conformations in *Arabidopsis* (33). It was noted that the active site of the open form appears unstable due to an incomplete structural model of the ligand-binding pocket (33). We therefore identified the crystal structures of FIN219–FIP1 in complexes with substrates such as JA, ATP, and preferred amino acids (Ile, Leu, Val, and Met) at a resolution of 1.54–2.25 Å, and with the FIP1 native-form structure at 1.65 Å (*SI Appendix*, Table S1).

The structures of FIN219–FIP1 in complexes with substrates JA, Ile, and ATP show two complex copies in an asymmetrical unit. The four structures reveal compact, horizontal molecular packing, with the N-terminal domain of FIN219 facing one of the FIP1 monomers (*SI Appendix*, Fig. S2*A*). FIN219 interacts with FIP1 via the rotatable C-terminal domain (T437–F575) that is sandwiched between the FIN219 N-terminal domain and FIP1 (Fig. 1*A*). This FIN219 fold differs from the structures of the AMP-bound closed form and ATP-bound open form (33–35). The hinge linker between the N- and C-terminal domains of

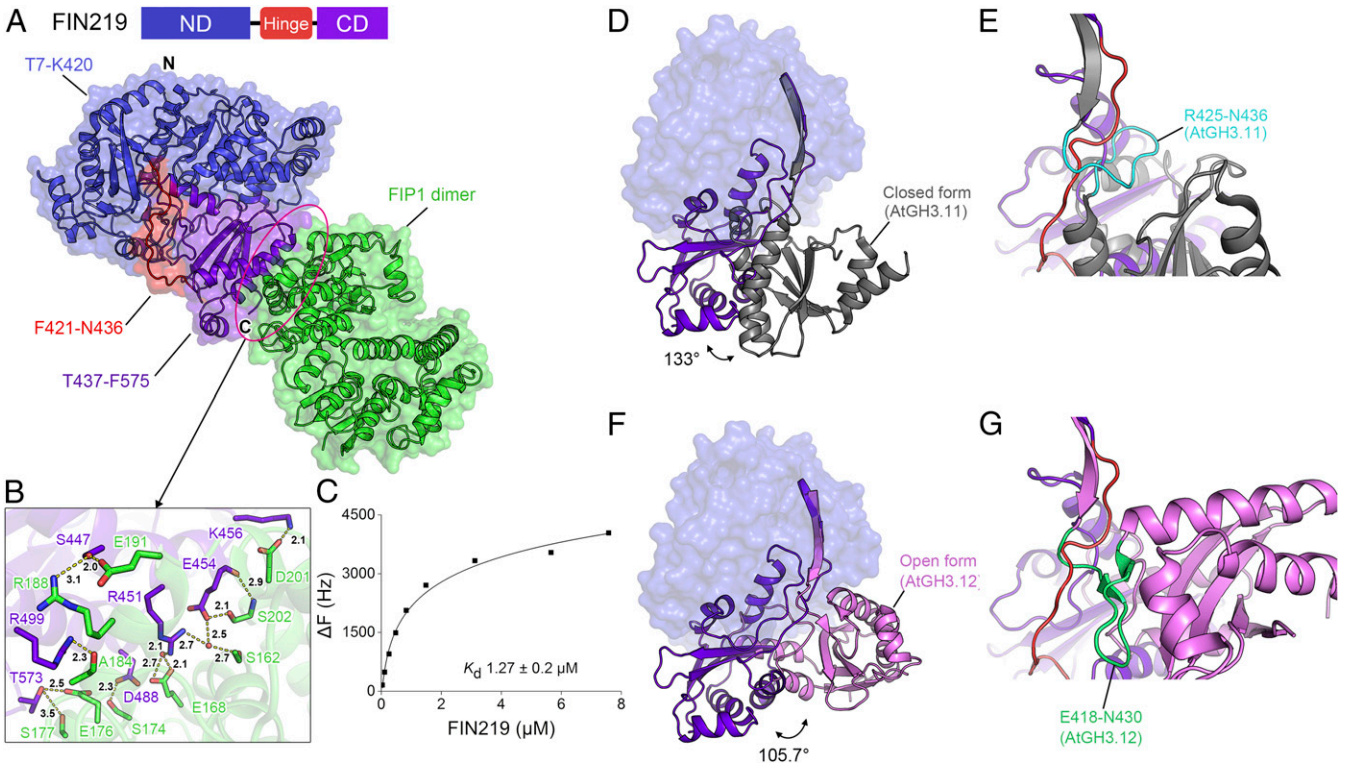

Fig. 1. Complex structure of FIN219–FIP1 and C-terminal domain switching between FIN219 and GH3 proteins. (*A*) Ribbon representation of crystal structure of the FIN219–FIP1 complex. The hinge linker, N-terminal domain (ND), and C-terminal domain (CN) of FIN219 are colored red, blue, and purple, respectively, and the FIP1 dimer is colored green. (*B*) Zoom-in view of the FIN219–FIP1 interface. Binding residues of the FIN219 C-terminal domain are shown as purple sticks, and FIP1 is shown as green sticks. Dashed yellow lines indicate a potential interaction network with bond lengths and water molecules shown as red spheres. (*C*) Determination of molecular interactions between FIN219 and FIP1 by QCM analysis. Data are representative of three independent experiments, and the error is calculated as SD. (*D*) Superposition of FIN219 between the complex form and closed form (PDB ID code 4EPL). The C-terminal domains of two conformations are shown as purple and gray ribbons with the indicated rotation angle. (*E*) Zoomed-in view of hinge linker between the N- and C-terminal domains in *D*. The hinge linkers of two conformations are colored red and cyan, respectively. (*F*) Superposition of FIN219 between the complex form and open form of AtGH3.12 (PDB ID code 4EWV). The C-terminal domain of two conformations is shown as a pink ribbon with the indicated rotation angle. (*G*) Zoomed-in view of the hinge linker between the N- and C-terminal domains in *F*. The hinge linker of AtGH3.12 is colored light green.

FIN219 reveals an unexpected conformation for domain switching (*SI Appendix*, Fig. S2 *D* and *E*), and we accordingly named it the complex form. On the interface, FIN219 and FIP1 show a helix–helix interaction: The helices α6–α8 of FIP1 contact the C-terminal helices α16–α17 of FIN219 (*SI Appendix*, Fig. S2*B*). The side chains R451 and K456 of FIN219 bind to E168 and D201 of FIP1 via an ionic interaction, and several residues supply hydrogen bonds that facilitate a stable interaction (Fig. 1*B* and *SI Appendix*, Table S2).

To investigate the biochemical relevance of the FIN219–FIP1 interaction observed in the crystal structures, we used a quartz crystal microbalance (QCM) technique to measure the dissociation constant (K_d) for binding affinity (36). FIN219 at various concentrations (0.2–1 mg/mL) was applied to immobilized FIP1, and we observed protein–protein interactions with a K_d of 1.27 ± 0.2 μM (Fig. 1*C* and Fig. 2*A*). These results confirm reported molecular interactions from in vivo experiments, which included yeast two-hybrid and coimmunoprecipitation (co-IP) assays (30). When the complex and closed forms of FIN219 structures [Protein Data Bank (PDB) ID code 4EPL] are superimposed on the N-terminal domain, DynDom server analysis reveals that the C-terminal region shows a structural reorientation, including a 133° rotation and 10-Å translation from the closed conformation (37) (Fig. 1*D*). The unwound hinge linker of FIN219 alters the C-terminal domain orientation and position. The affected C-terminal domain inserts into the groove at the bottom of the N terminus at the helices α20 and α21, creating a more occluded conformation of the active site than the closed form of FIN219 (Fig. 1*E*). In contrast, the C-terminal region of the open form of AtGH3.12 (PDB ID code 4EWV) shows another orientation relative to FIN219, with a rotation of 105.7° and 5.7-Å translation in comparison to the FIN219-complex form. This conformation exposes a ligand-binding entry in the bottom of the N terminus, which is used for substrate assembly (Figs. 1 *F* and *G*). We found that FIN219 and AtGH3.12 could only be superimposed with a backbone root-mean-square deviation of 1.66 Å across 274 Cα atoms in the N-terminal regions. This discrepancy is due to an inadequate crystallographic model of the open form of AtGH3.12, and particularly to the residues near the ATP-binding site. Overall, the structure of FIN219 in the FIN219–FIP1 complex shows that it is in a stable state after binding with FIP1.

Structural and Functional Characterization of FIP1. FIP1 possesses a canonical, homodimerized GST protein fold. It consists of two GST-binding sites and shows a cashew-shaped profile in both the FIN219–FIP1 and FIP1 structures (27, 28) (*SI Appendix*, Fig. S3*A*). The dimer interface of FIP1 is composed of the helices α3 and α4 joined by a short strand. One monomer is packed against the equivalent helices in another monomer within a central twofold symmetry (*SI Appendix*, Fig. S3*B*). Sequence alignment and structural comparison (38) (*SI Appendix*, Fig. S4) show that E76, R92, and R96 are highly conserved, can contact each other, and form ionic interactions. N69 and A93 provide hydrogen bonds for dimerization (*SI Appendix*, Fig. S3*C*). Each FIP1 monomer consists of 10 helices, with a triple-helix bundle within helices α4–α6. Four β-sheets are sandwiched between helices α1 and α3 (*SI Appendix*, Fig. S3*D*). The substrate GSH shows a clear F_o-F_c map contour in the ligand-binding pocket of FIP1 and interacts with conserved K40, E66, and S67 (Fig. 2*B*). Having observed this GST fold, we performed a transferase assay to detect the product formation of [S-(2,4-dinitrobenzyl)glutathione (GS–DNB)] at A_{340}. FIP1 showed lower GST activity than *Schistosoma japonicum* GST (SjGST), a GST protein expressed using the pGEX 4T-1 vector (Figs. 2 *C* and *D*). Apart from the slightly shifted helices α4–α6, the FIN219 binding did not appear to alter the FIP1 overall conformation (*SI Appendix*, Fig. S3*E*). Surprisingly, some of the FIN219-binding residues were also highly conserved in GSTs of other species, particularly the residues E168, R188, and D201 (*SI Appendix*, Fig. S4). This conservation is consistent with similar regions of tau-class GSTs, demonstrating the importance of conserved residues in this class for the specific recognition of FIN219.

Insights into the Active Site Architecture of the Complex-Form FIN219. The FIP1 binding altered the FIN219 C-terminal domain orientation. As a result, the entrance of ~250 Å^2 at the active site was blocked by the helices α20 and α21 of the C-terminal region (Fig. 3*A*). The helix α20 in the rotated C-terminal domain of FIN219 inserts into the cavity of the active site, structurally pushing the

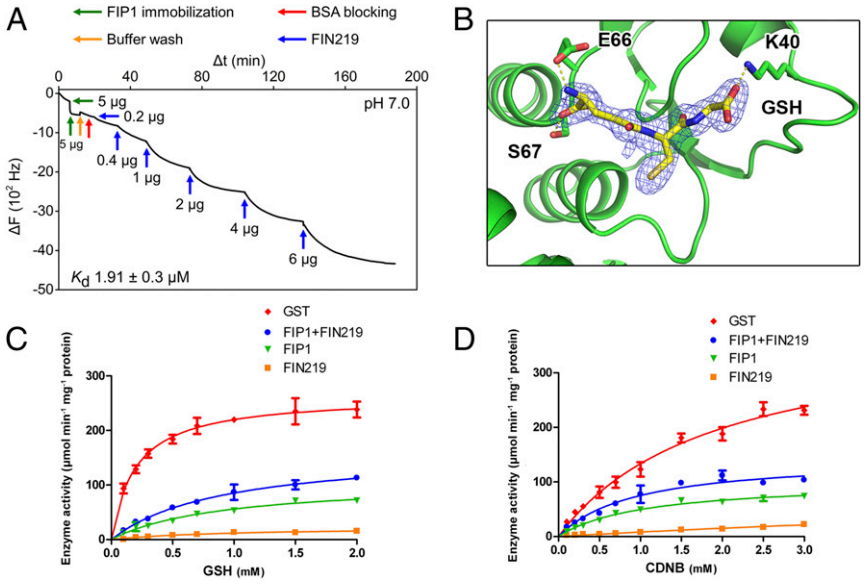

Fig. 2. FIN219–FIP1 binding assay and characterization of GST enzymatic activity of FIP1. (*A*) Interaction of FIN219–FIP was detected on the QCM. The reduced frequency refers to the increased mass by molecular binding, and the K_d value was calculated from each point of protein injection. (*B*) Ribbon diagram of the FIP1 active site with GSH shown as yellow sticks contoured at 5σ from a F_o-F_c map. Spectrophotometric assays for GST activity determination with the specific substrates GSH (*C*) and CDNB (*D*) are shown. FIP1 catalyzed the conjugation of L-GSH to CDNB through the thiol group of the GSH, and the derivative GS-DNB was measured (A_{340}). The activities of SjGST and FIN219 are shown as positive and negative controls, respectively.

bound ATP into the interior of the active site. Thus, the adenine ring moiety is oriented toward JA and binds to the K557 of helix α21 via γ-phosphate. The omit map illustrates a definite electron density of bound JA, isoleucine, and ATP in the middle of the reconstructed active site (Fig. 3*B*). The isoleucine substrate binds with water-mediated hydrogen bonds directly to the E533 carboxyl group, as well as to the A165, K530, and E533 side chains. Remarkably, residues F220, V222, I304, H328, and W336 are involved in the apolar binding to the cyclopentane ring of JA, whereas polar binding occurs between H328 and the JA acyl group (Fig. 3*C*). Additionally, L124, F125, and W336 provide a hydrophobic pocket for the pentenyl tail (*SI Appendix*, Fig. S5*A*). The comparison between the active sites of the complex form of FIN219 and closed forms reveals that, in the closed form, JA-Ile departs from the hydrophobic pocket and shifts to a larger pocket near the active site entry. The carboxyl group of the Ile moiety is oriented toward S100, S101, and S333 (33) (*SI Appendix*, Fig. S5*B*). Given this difference and the uniqueness of JA pentenyl tail docking, we expected that Trp336 would play an important role in hormone selection; this amino acid is not a conserved residue in other GH3 proteins. At the ATP binding site, T121, A165, and G331 provide hydrogen bonds with adenosine and N168, S98, and K557 interact with α-, β-, and γ-phosphate, respectively (Fig. 3*D*). Stacking W336 with the adenine ring allows ATP to assume a shrimp-shaped structure, and the phosphate group inclines toward the acyl-adenylate motif I (S_{98}LSSGT$_{103}$ in FIN219 and S_{95}SGTSG$_{100}$ in AtGH3.12) (11), although the position of ATP is altered. K557 in the rotated C-terminal domain of FIN219 makes contact with the ATP phosphate tail and acts as a conserved lysine in the canonical Walker A motif [GXXXXGK(T/S)]. A comparison of the active sites between FIN219 and the closed form of AtGH3.12 shows that the configurations of catalytically important residues are different. In particular, there is a 15-Å molecular shift between ATP and AMP in each structure (Fig. 3*E*). The ATP binding in the FIN219 is displaced into the residues of the helices α5, α6, and α21 in the C-terminal domain instead of sheets β1, β7, β12, and β13 in AtGH3.12, as previously indicated (33). These structural observations help to explain how domain rotation occurs in FIN219. They show the protein complex in an unanticipated conformation leading to reorganization of the substrate-binding site, which may aid the nucleophilic attack during catalysis. To substantiate this theory, we superposed the FIN219 structure with open-form AtGH3.12 and closed-form VvGH3.1 (PDB ID code 4B2G) from grapevine (*Vitis vinifera*) (39). An ATP analog, α,β-methylene adenosine 5′-triphosphate (AMPCPP) in the

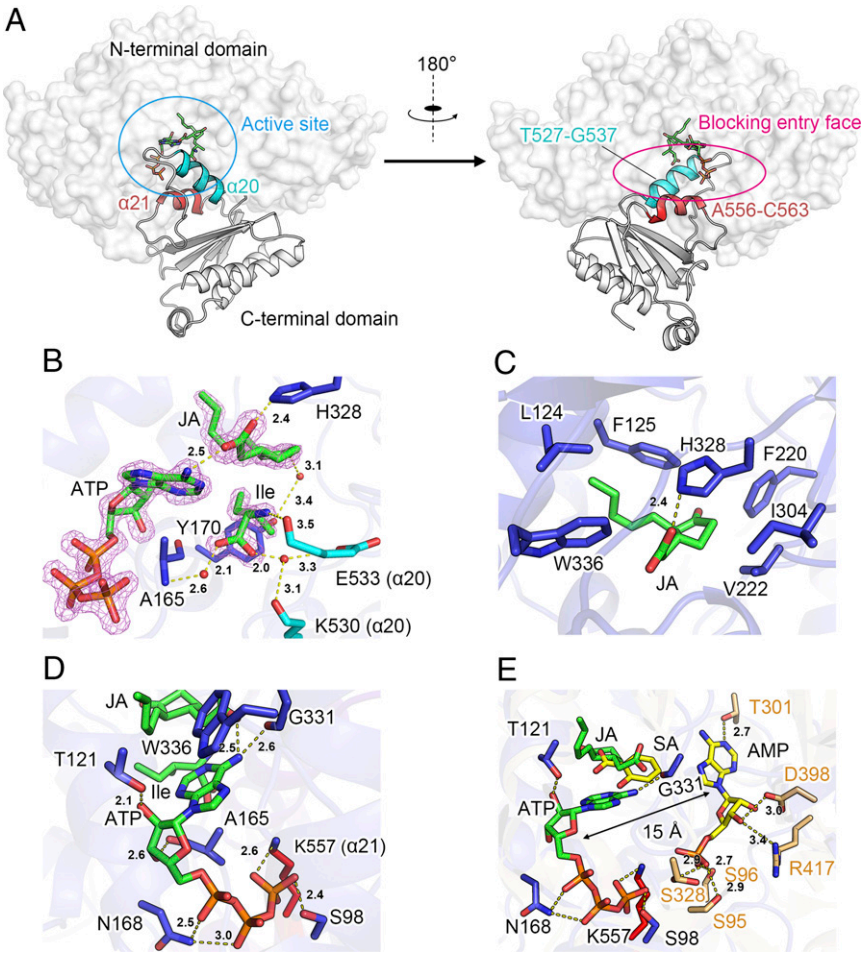

Fig. 3. Insights into the active site of complex-form FIN219. (*A*) Two views of the FIN219 complex-form structure. The semitransparent N-terminal domain shows a buried active site, and the helix α20 and helix α21 of the C-terminal domain nearby substrates are shown as cyan and red ribbons, respectively. (*B*) Residues at the jasmonic acid (JA) and isoleucine (Ile) binding site of FIN219 are shown as blue (N-terminal) and cyan (α20) sticks, and all substrates are contoured at the 6σ F_o-F_c map before being modeled in. Dashed lines with bond lengths are indicated, and waters are shown as red spheres. ATP is represented near JA and Ile, and it interacts with JA through the adenine ring. (*C*) Hydrophobic pocket of JA and surrounding side chains are shown as sticks. (*D*) Residue side chains at the ATP binding site of FIN219. (*E*) Structural superposition of the FIN219 and AMP-bound closed-form AtGH3.12 (PDB ID code 4EQL). Key residues and bound substrates of AtGH3.12 are shown as light orange and green sticks, respectively, with the indicated bond lengths. The molecular distance between ATP in FIN219 and AMP in AtGH3.12 is labeled.

AtGH3.12 structure, shows a similar binding position to the inhibitor adenosine-5′-[2-(1H-indol-3-yl)ethyl]phosphate (AIEP) in the VvGH3.1 structure. The helix α20 of FIN219 seizes both the primordial AMPCPP- and AIEP-binding sites in AtGH3.12 and VvGH3.1, respectively (*SI Appendix*, Fig. S5 *C* and *D*). This demonstration provides an explanation for the difference between the substrate-binding mode of FIN219 and other GH3 enzymes.

FIN219 Activation and Insights into Substrate Binding of Acyl-Adenylate Motifs. Having obtained the structural information, we proceeded to investigate the importance of acyl-adenylate motifs for FIN219 substrate binding. We also attempted to establish whether the interaction with FIP1 improves FIN219 adenylation activity. We used the Taussky–Shorr method to measure the amount of pyrophosphate released from ATP by the FIN219 enzyme reaction (40), with ATP as a specific activity target. In Michaelis–Menten kinetics, the adenylation activity per mole of FIN219–FIP1 was approximately double the adenylation activity per mole of FIN219 alone (Fig. 4*A* and *SI Appendix*, Table S3). The JA response-defective JAR1-1 (S101F) protein showed severely reduced activity. This observation corresponds to our findings that FIP1-mediated FIN219 domain reorientation increases the rate of JA-Ile biosynthesis. It also suggests that S101 of the acyl-adenylate motif I is critical for the acyl-adenylation half-reaction. To confirm these biophysical properties of enzyme–substrate complexes, we performed a QCM experiment to examine the catalytic reaction directly and to determine the substrate-binding mode. The QCM data showed a series of trough curves, with each ATP concentration plotted in a linear regression in the kinetic mode (Fig. 4 *B* and *C*). ATP showed a remarkable binding affinity to the FIN219–FIP1 complex. B_{max} and V_{max} for the complex were, respectively, twofold and 2.3-fold greater than for FIN219 alone (Fig. 4 *B* and *C* and *SI Appendix*, Table S3). These results and our structural analysis do indeed confirm that the catalytic efficiency of FIN219 is improved via the FIP1 interaction. The FIN219–FIP1 complex also showed a higher binding affinity to JA than FIN219 alone, with lower K_d values (Fig. 4 *D*–*G*). Interestingly, neither ATP nor isoleucine could bind directly to FIN219 or to the

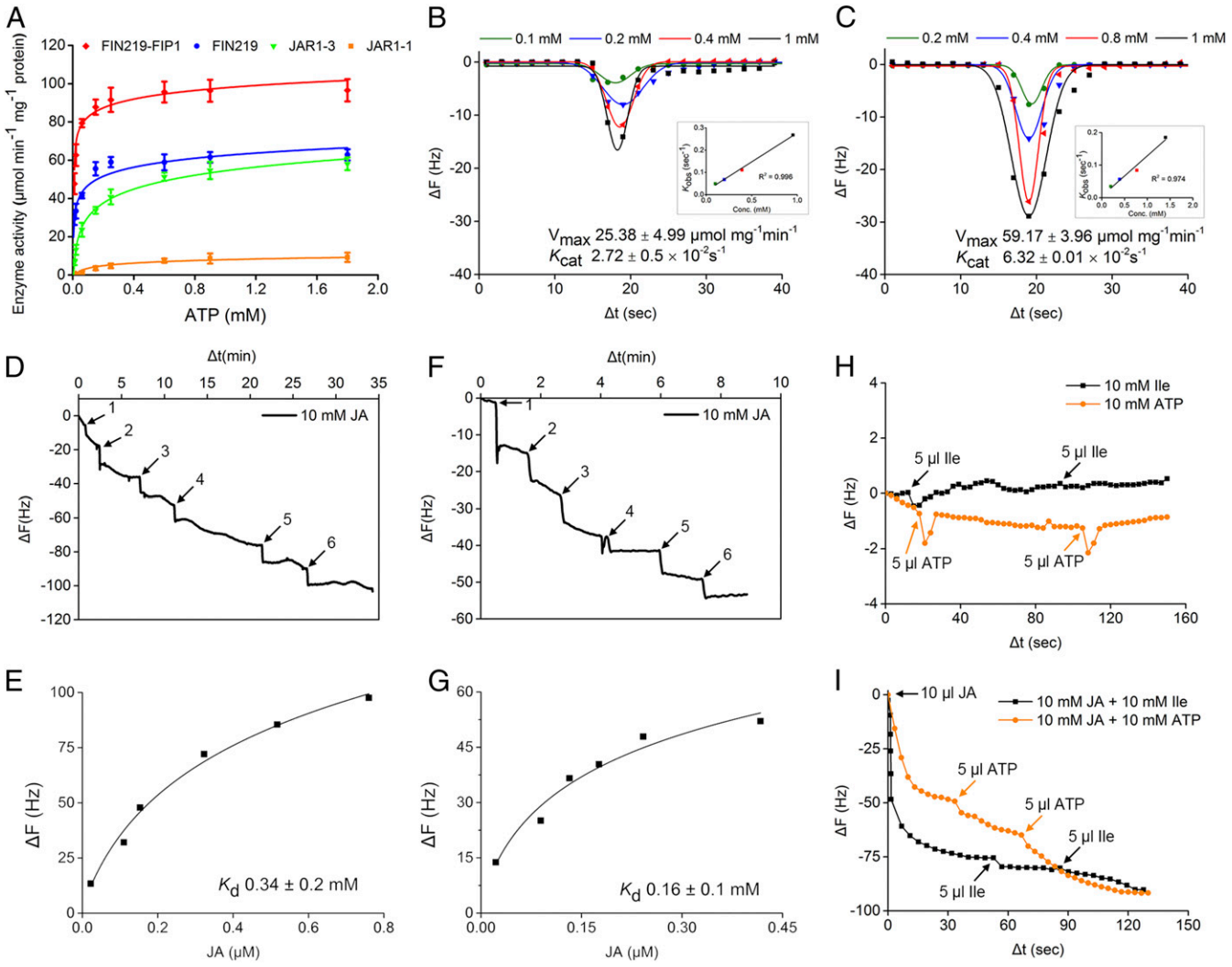

Fig. 4. Kinetics and QCM assay for FIP1-enhanced FIN219 activity and FIN219 substrate binding priority. (*A*) Adenylation activity assay of FIN219, FIN219–FIP1 complex, and mutants. Data are represented as inorganic phosphorus measurements decomposed from pyrophosphate of the adenylation product at A_{650}. (*B* and *C*) QCM kinetics assay of adenylation of FIN219 (*B*) or the FIN219–FIP1 complex (*C*). ATP was titrated to FIN219-immobilized (*B*) or the FIN219–FIP1 complex-immobilized (*C*) sensor with different concentrations. The kinetic parameters V_{max} and K_{cat} are indicated. The insets are the linear regression of different ATP concentrations for FIN219 (*B*) and the FIN219–FIP1 complex (*C*) with $R^2 = 0.996$ (*B*) and 0.974 (*C*), respectively. (*D* and *E*) Binding assay of FIN219 with JA in raw frequency (*D*) and plotted (*E*) curves. (*F* and *G*) Binding assay of the FIN219–FIP1 with JA in raw frequency (*F*) and plotted (*G*) curves. (*H* and *I*) Binding assay of FIN219 (*H*) and the FIN219–JA complex (*I*) with responsive substrates. All data are representative of three independent experiments, and the error is calculated as SD.

FIN219–FIP1 complex unless JA had been bound first (Fig. 4 *H* and *I*). This observation suggests that JA binding is essential for other substrate recruitment and for further reactions. Indeed, the prior binding of JA to FIN219 plays an important role in JA-Ile synthetase activity. We therefore highlight the increase in catalytic efficiency of complex-form FIN219 during conformational switching.

Implications of FIN219 Binding Specificity for Different Amino Acid Substrates. JA derivatives with different amino acids on the acyl moieties are essential for plant development. To examine substrate preference, we cocrystallized FIN219–FIP1 proteins with three other preferred amino acids (Leu, Val, and Met) identified in previous studies (33, 41). We determined the protein–ligand complex structures at resolutions of 1.6–2.3 Å and labeled these data using the names of cocrystallized substrates, respectively (e.g., JA–Ile–ATP refers to the FIN219–FIP1 complex with ligands JA, isoleucine, and ATP) (*SI Appendix*, Table S1). The examined active sites, S332, S333, and W336, had notably reoriented side chains with bound amino acid substrates. However, the configurations of the JA–ATP structures were the same as the configurations in JA–Ile–ATP (Fig. 5 *A*–*C*). ATP shows a shifted ribose, phosphate tail, or different orientation of adenine in JA–Leu–ATP and JA–Val–ATP (Fig. 5 *D* and *E*). The orientation of the adenine base of ATP in the JA–Met–ATP structure is opposite to the orientation of the adenine base of ATP in the JA–Ile–ATP structure, and the repositioned Trp336 loses its stacking capability with the adenine ring of ATP and the pentenyl tail of JA (Fig. 5*F*). This discrepancy shows that the preference for the amino acid substrate is determined by the structure discriminating between apolar substrates (Ile, Leu, Val, and Met) and polar amino acids at the hydrophobic binding site. This phenomenon further affects the architecture of the bound ATP, as well as catalytic efficiency. We also found that S332 and S333 of the acyl-adenylate motif II ($Y_{330}GSSE_{334}$) (11) are adjacent to the ATP phosphates, which may be important for adenylation and thioesterification reactions. We also soaked various complex crystals with an Mg^{2+} cofactor and determined its locality. The electron map of Mg^{2+} in two complexes of JA–ATP–Mg revealed that it is located near the ATP γ-phosphate, and that S98 played a major role in the contact between ATP and Mg^{2+} (*SI Appendix*, Fig. S6 *A* and *B*). Mg^{2+} also binds to neighboring amino acid substrates or JA in various complex structures without ATP (*SI Appendix*, Fig. S6 *C*–*F*).

Discussion

A previous study found that both FIN219 and FIP1 are involved in FR light signaling (30). FIP1 was found to interact with the FIN219 C-terminal region in the yeast two-hybrid and pull-down assays, and antibodies in the co-IP assay in a *fin219* null mutant background did not detect FIP1 proteins (30). Furthermore, FIN219 activates systemic synthesis of bioactive JAs in *Arabidopsis* (22). In this study, we determined the regulatory roles of FIN219 and FIP1 whether in FR light signaling or in the JA-response pathway, and we obtained high-resolution structures of the FIN219–FIP1 complexes bound to their target substrates. We then provided functional and structural evidence for FIP1-mediated regulation of FIN219 activity. Further, we showed that the FIP1-regulated FIN219 conformational change is crucial for improving JA-Ile biosynthesis, which may be directly linked to the level of JA-mediated plant defense responses (22). Based on these results, we present a working model for interpreting the FR light-coupled JA response (Fig. 6). According to previous research, GH3 proteins may recruit acyl acids and amino acids in the closed-form structure (33). The change from the closed form to the open form may occur in the presence of ATP, and this folding is the main conformation for the adenylate-forming reaction in the ANL (acyl-CoA synthetases, NRPS adenylation domains, and luciferase enzymes) superfamily of adenylating enzymes (42). Thioesterification is catalyzed when the enzyme changes back to the closed form, and the enzyme then completes a catalytic cycle and is available for the next reaction (10). Here, the FIP1-mediated new conformation of FIN219 provides another catalytic strategy, and this strategy is crucial for reciprocal cross-talk between FR light signaling and JA response

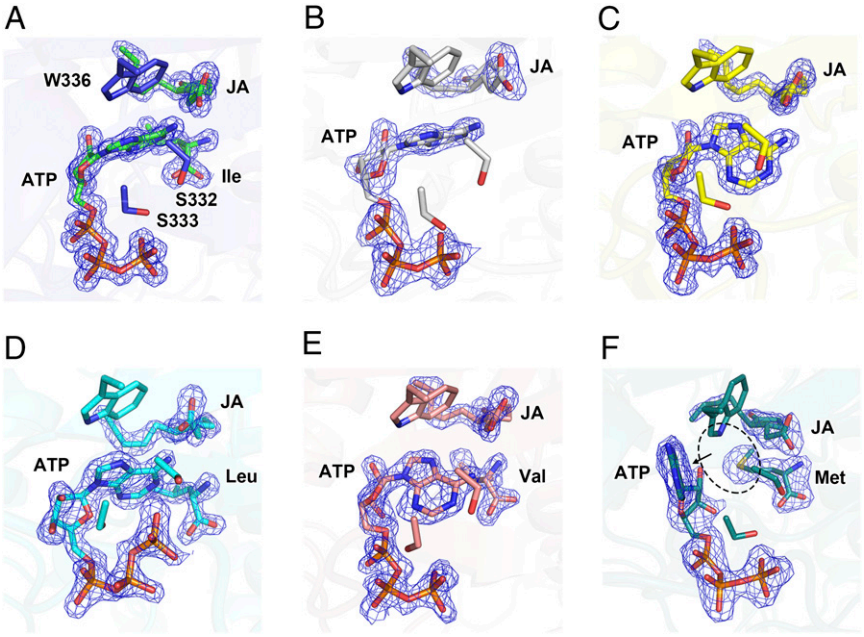

Fig. 5. Acyl-adenylate motif II in the FIN219 active site influenced substrate-specific activation. Stick representation of ligands JA–Ile–ATP (*A*), JA–ATP (*B*), JA–ATP–Mg (*C*), JA–Leu–ATP (*D*), JA–Val–ATP (*E*), and JA–Met–ATP (*F*) with critical residues S332, S333, and Trp336 participating during the adenylate-forming reaction and thioester-forming reaction in the complex-form FIN219. View of each substrate contoured at 5σ from a F_o-F_c map without a ligand structure during refinement. JA–Ile–ATP (*A*) and JA–ATP (*B*) did not differ in ligands, and the adenine of ATP in JA–ATP–Mg (*C*), JA–Leu–ATP (*D*), and JA–Val–ATP (*E*) shows an altered placement. (*F*) Residue Trp336 JA–Met–ATP reveals a varied aromatic ring position, which affects the adenine of ATP orienting to an opposite direction in the active site.

(43). Our structural data confirmed that the complex conformation of FIN219 could simultaneously accommodate JA, amino acids, and ATP binding at the active site; the occluded entrance structure; and the ATP repositioning (Fig. 6). There are also indications that the conformation might prevail after substrates attach, because the entrance of the ligand-binding pocket is blocked by the C-terminal domain (Fig. 3*A*). For this phenomenon to occur, the helices α20 and α21 must be in close proximity to isoleucine and ATP, which enables the repositioned ATP to bind to the acyl-adenylate motif I (*SI Appendix*, Fig. S7*A*). The reaction that produces adenylate may be facilitated by S332 and S333 in motif II, which enables the nucleophilic attack by interacting with the α-phosphate of ATP and JA carboxylate when adenylate is produced (*SI Appendix*, Fig. S7*B*). The isoleucine further conjugates to the acyl group of the JA-AMP intermediate when thioester is produced (*SI Appendix*, Fig. S7*C*). Subsequently, JA-Ile repositions itself at the entry of the active site and binds to S100 and S101 with the carboxyl group of isoleucine moiety (*SI Appendix*, Fig. S7*D*).

Our data indicate that during biosynthesis of JA-amino acid, the FIN219–FIP1 causes a local change in the C-terminal domain that further affects the position of ATP with respect to K557 in helix α21. The increased adenylation rate may be caused by altered efficiency of the formation of hydrogen bonds in the ATP motif I and when the more compact substrate binding pocket is rebuilt. Perhaps our most surprising finding, however, is that the previously characterized K435 required in the ATP binding was replaced by K557. It is predominantly located in the reoriented C-terminal gate for ATP phosphate tail binding, fulfilling a function similar to lysine in the Walker A motif [GXXXXGK(T/S)]. The repositioned ATP has a more compact shape and is closer to JA, a position more suitable for nucleophilic attack at the ATP α-phosphate during the adenylation half-reaction. This phenomenon also explains why the complex form of FIN219 is more active than the original conformation. The amino acid substrate-binding sites of GH3 proteins have not previously been accurately identified. Our structural data demonstrate how the amino acid substrates bind to the active site of the complex form of FIN219 and show the different binding properties of various amino acids. Unexpectedly, we found that biosynthesis of JA derivatives may depend on the structural binding stability of ATP, rather than on the ligand-binding selectivity of amino acids when they attach to substrates. In contrast to the clear contour of electron density of the JA–Ile–ATP complex, the rough-contoured JA–Met–ATP structure suggests it is in a locally unsteady state. The density map of the adenine ring of ATP noticeably leaves the JA acyl moiety (Fig. 5*F*). Previous analysis by TLC assay has indicated that methionine has the lowest binding affinity to FIN219 (16). Our structural data show that recruiting less favorable amino acids may interfere with the ability of ATP to bind to FIN219. These results corroborate the results of gas chromatography-mass spectrometry quantification of JA derivatives: In *Arabidopsis* seedlings, JA-Ile predominates (15, 41). Further research is required to identify whether FIN219 has a specific recognition motif for amino acid selectivity.

Two decades ago, the first X-ray structure of an adenylate-forming enzyme, *Photinus pyralis* luciferase, was presented (44). The firefly luciferase structure and other structures reported for this family have a similar fold formed by a large N-terminal domain and a smaller C-terminal domain. Three main subfamilies, namely acyl-CoA synthetase, the nonribosomal peptide synthetase adenylation domains, and the luciferase enzymes,

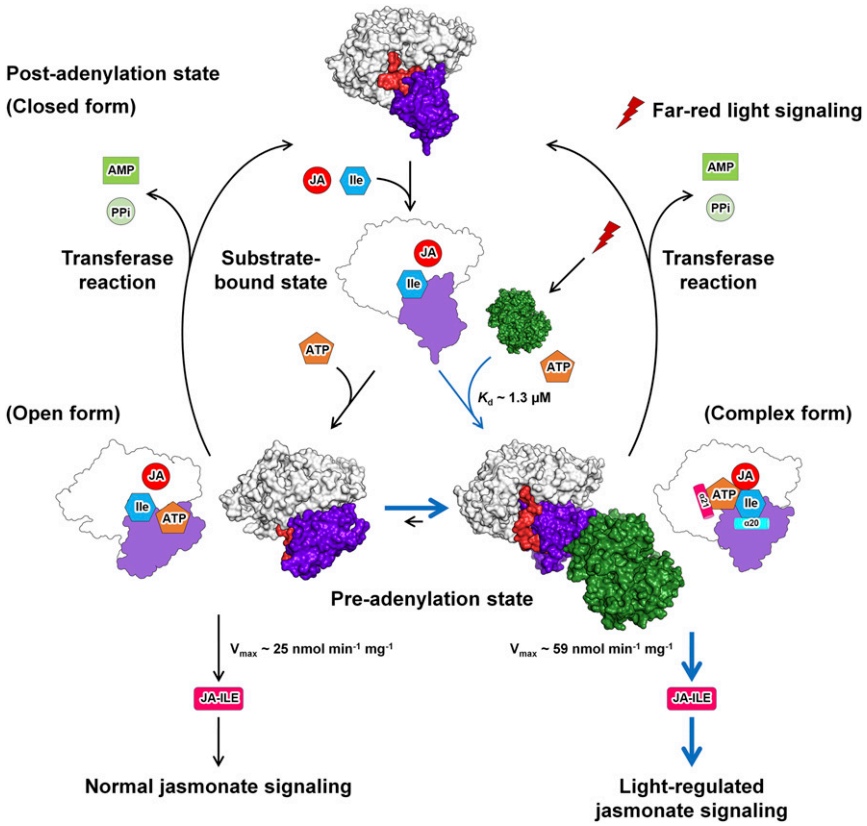

Fig. 6. Proposed model of FIN219 conformational change and its functional consequences. The closed form is proposed as a major postadenylation state for JA and isoleucine recruiting, and the open form is a definite ATP-binding fold. Furthermore, FIP1 is up-regulated under phytochrome A-mediated FR light signaling, and interacts with FIN219 for higher JA-amino acid catalytic activity. Therefore, we proposed that the FIN219–FIP1 protein complex plays as an important role in signaling cross-talk between FR light and JA for triggering the light-enhanced JA response.

were integrated into the new ANL superfamily of adenylating enzymes (42). The majority of the invariant residues conserved in this family are clustered on the surfaces of the domain–domain interfaces, suggesting that this site is the location of the catalytic site (42). The conserved residues compose three motifs: motif I (S/T-S/T/G-G-S/T-S/T), motif II (Y-G/W-X-S/T-E), and motif III (Y-X-X-G-D) (42). These motifs are distributed throughout the ANL superfamily and are crucial for the enzymatic activity of these proteins (42). Hence, we illustrated the different structures of FIN219 and various adenylating enzymes of the ANL superfamily in adenylation, intermediate, and thioesterification conformations (42) (*SI Appendix*, Fig. S8 *A–C*). The adenylation and thioesterification conformations clearly correspond to the open form and the closed form due to their structural appearances and involved the catalytic state. Although the structural alignments were obstructed because the N-terminal domain of FIN219 is obviously larger than benzoate-CoA ligases, acetyl, or long-chain fatty acyl-CoA synthetase, the superimposed structures nevertheless revealed that the C-terminal domains of all three conformations differ distinctly from the complex form of FIN219 (*SI Appendix*, Fig. S8 *A–C*). This distinct conformational effect confirms that the FIN219 activity is regulated by FIP1 interaction. There are no previous reports of structural and functional alterations of adenylating enzymes caused by protein–protein interactions for this superfamily.

The mechanisms of FIN219 and FIP1-regulated JA-Ile biosynthesis during FR light signaling remain unclear because FIN219 may interact with other GST proteins. We demonstrated that the residues from the FIN219-binding interface with FIP1 are consistent with the conserved regions of FIP1 orthologs (*SI Appendix*, Fig. S4). In particular, the residues E168, R188, and D201 are similar to the residues in other GSTs of the tau class from various species (*SI Appendix*, Fig. S4). Interestingly, we also noticed that FIN219 interacts with non–tau-class GSTs. Molecular binding between FIN219 and SjGST derived from *S. japonicum* has been observed during protein purification. SjGST expressed from the pGEX4T-1 vector originally fused at the N terminus of FIN219, and it binds to FIN29 immediately after the thrombin-cleavage reaction. Protein-binding behavior was also observed through size-exclusion chromatography, where incubation of the FIN219–SjGST interaction resulted in a peak shift of the SjGST elution volume (*SI Appendix*, Fig. S9*A*). We also succeeded in crystallizing and determining the FIN219–SjGST complex structure (*SI Appendix*, Fig. S9 *B* and *C*). FIN219–SjGST shows a similar binding conformation and interface to FIN219–FIP1 (*SI Appendix*, Fig. S9 *D* and *E*), but the binding residues from the FIN219-interacting interface with SjGST are dramatically different from the binding residues of FIP1 (*SI Appendix*, Fig. S9*F*). SjGST has been characterized as a mu-class GST, and its function is to conjugate GSH with toxic secondary products from membrane lipid peroxidation (45). However, mu-class GSTs are absent in *Arabidopsis*. These results suggest that a network of complicated protein–protein interactions exists between FIN219 and the GST superfamily.

The GST family proteins are involved in numerous reactions, including detoxification and reduction of oxidative stress. In plants, excessive light leads to the production of reactive oxygen species (ROS) and activates the defense system of antioxidant enzymes, such as superoxide dismutase, ascorbate peroxidase, and GST. The process provides protection against ROS produced during normal cellular metabolic activity and photosynthesis (46). The excess light-induced ROS defense mechanism is also linked to JA signaling through transcriptional regulation (43). Previous research revealed that overexpression of members of the *Arabidopsis* GST superfamily in *Escherichia coli* resulted in 25 of the 28 GST tau (U) proteins (GSTUs) causing an aberrant accumulation of acylated GSH thioesters in vivo, a perturbation that was not observed with other GST classes (47). In particular, the study demonstrated that GSTU members catalyzed the S-glutathionylation of 12-oxo-phytodienoic acid (OPDA), an early bio-synthetic precursor of JA (28, 47). Further research is required to determine whether FIP1 plays a role in other regulatory mechanisms in jasmonic acid signaling, such as preventing epimerization of the active (+)-7-iso-jasmonoyl-L-isoleucine attaching to the inactive (−)-jasmonoyl-L-isoleucine. Furthermore, the function of the FIN219 acyl-adenylate motif III ($Y_{401}RLGD_{405}$) and the regulatory mechanism of the interactions with other GSTs also require additional investigation. Our determination of the crystal structures of the FIN219–FIP1 complex establishes a GH3 structural framework allowing an understanding of the dual affinity of jasmonoyl-isoleucine synthetase. These structures also demonstrate how light signaling may affect JA biosynthesis under continuous FR light conditions and further enhance JA signaling in *Arabidopsis*.

Materials and Methods

Cloning, Expression, and Purification of FIN219 and FIP1. The cDNAs of full-length *Arabidopsis thaliana* FIN219 (AT2G46370), JAR1-1 (S101F), and JAR1-3 (E334K) were cloned into the pGEX-4T-1 vector (GE Healthcare) with a GST tag at the N terminus. The cDNAs of full-length *A. thaliana* FIP1 (AT1G78370) were cloned into the pRSET-B vector (Invitrogen) with a hexahistidine tag (6×His tag) at the N terminus. The expression vector was transformed into *E. coli* BL21(DE3) cells, grown at 37 °C in LB medium until the optical density achieved 12 at 600 nm. The 3% (vol/vol) ethanol was added during expression for inducing the endogenous chaperones of *E. coli* to assist the recombinant protein folding (48). The expression of GST-FIN219 proteins was induced by 0.1 mM isopropyl β-D-1-thiogalactopyranoside (IPTG) for 18 h at 16 °C. GST-JAR1-1 and GST-JAR1-3 were expressed in *E. coli* BL21(DE3) cells, grown at 37 °C for 4–6 h in LB, and induced overnight with 0.1 mM IPTG at 25 °C. His-FIP1 was expressed in *E. coli* BL21(DE3)pLysS cells, grown at 37 °C for 2 h in LB, and induced for 2 h with 0.1 mM IPTG at 37 °C. All cells were collected by centrifugation at 9,820 × *g* for 30 min at 4 °C, and then resuspended and lysed in wash buffer A [20 mM Hepes (pH 7.5), 0.2 M NaCl, 1 mM DTT, 1 mM EDTA, 0.1 M glycine, 0.3 M sucrose, 10% (vol/vol) glycerol] for GST-FIN219, GST-JAR1-1, and GST-JAR1-3 and in wash buffer B [50 mM Tris·HCl (pH 7.5), 0.5 M NaCl, 50 mM imidazole] for His-FIP1. Cells were lysed by sonication, and the cell debris was removed via centrifugation at 27,200 × *g* for 30 min at 4 °C. The filtered supernatants of GST-FIN219, GST-JAR1-1, and GST-JAR1-3 were applied to 5 mL of a GSTrapFF (GE Healthcare) column, and filtered supernatant of His-FIP1 was applied to 5 mL of a HisTrapFF (GE Healthcare) column. On-column cleavage of GST-fusion proteins was performed by a thrombin reaction for 2 h at room temperature. Recombinant proteins were then separated from GST-tag and eluted with the elution buffer, including wash buffer A and 10 mM GSH. The redundant GSH was removed from eluted FIN219 proteins by a HiTrap Desalting (GE Healthcare) column. FIN219 protein was further purified by size-exclusion chromatography and applied to a Superdex 200 (GE Healthcare) column with wash buffer A. The fractions of elution peaks containing monomeric FIN219 proteins were pooled and further concentrated to 10 mg/mL using a 50-kDa centrifuge tube (Amicon Ultra-15 Centrifugal Filter; Merck Millipore) and then stored at 4 °C. His-FIP1 was washed with wash buffer B and eluted with the elution buffer, including 50 mM Tris·HCl (pH 7.5), 0.5 M NaCl, and 500 mM imidazole. The redundant imidazole was removed from eluted FIP1 by a HiTrap Desalting column, concentrated to 10 mg/mL using a 10-kDa centrifuge tube (Amicon Ultra-15 Centrifugal Filter), and then stored at 4 °C.

Crystallization, Data Collection, Structure Determination, and Refinement. Crystals of the FIN219–FIP1 complex and FIP1 were initially obtained with the Crystal Screen kit (Hampton Research) under the same conditions (crystal screen 1, no. 22) and grown at 23 °C by the hanging-drop vapor diffusion method. FIN219 and FIP1 proteins were pooled at an equal molar ratio and concentrated to 8 mg/mL for crystallization. One microliter of FIN219–FIP1 protein was mixed with 1 μL of reservoir solution containing 0.2 M sodium acetate trihydrate, 0.1 M Tris·HCl (pH 8.5), and 30% (wt/vol) PEG 4000. Ten millimolar (±)-jasmonic acid (J2500; SIGMA) and 10 mM GSH were applied to the protein drops for cocrystallization. One microliter of 10 mg/mL FIP1 protein was mixed with 1 μL of reservoir solution as described previously. Ten micromolar GSH was applied to the protein drops for cocrystallization. Crystals of the maximal sizes of FIN219–FIP1 and FIP1 were obtained after 3 d by the sitting-drop method in a 1:1 protein/solution ratio (total volume of 10 μL) under 0.8 and 0.3 M sodium acetate trihydrate, respectively. Crystals of FIN219–FIP1 were then soaked in ligand solutions containing the reservoir solution and different combinations of (10 mM each) of Ile, Leu, Val, Met, ATP, and $MgCl_2$ for 24 h. All data were collected at beamline 13C1 of the Taiwan Light

Source at the National Synchrotron Radiation Research Center (Hsinchu, Taiwan). The X-ray diffraction data were recorded through a Rayonix MX-300 CCD detector and collected by means of Blu-Ice software (49). Data were indexed, integrated, and scaled with use of the HKL2000 package (50).

All FIN219–FIP1 and FIP1 diffraction data were solved on the PHENIX platform (51), and all showed a twofold axis pseudomerohedral twinning (JA–Ile–ATP, JA–Leu, JA–Leu–ATP, JA–Val–ATP, and JA–ATP–Mg) (52) or three equivalent pseudomerohedral twin laws (JA–Ile–Mg, JA–Leu–Mg, JA–Val–Mg, JA–Met–ATP and JA–ATP) detected by phenix.xtriage. The structures of FIP1 and FIN219 were solved by molecular replacement with Phaser (51, 53) using the *Glycine max* GSTU4-4 monomeric model (PDB ID code 2VO4) (29) and closed form of the FIN219 model (PDB ID code 4EPL) (33) minus ligands as templates. The molecular replacement solutions for FIN219 structure revealed that neither the closed-form FIN219 nor open-form AtGH3.12 (PDB ID code 4EWV) was reasonable to phase the new complex conformation of FIN219. Moreover, the simultaneous searches of molecular replacement of the FIN219 N- or C-terminal region with FIP1 also failed because of severely biased phasing from translational noncrystallographic symmetry and twinning. For resolving the complex architecture of FIN219, we indexed and scaled all complex data as space group P1; the model of the C-terminal domain, including a hinge linker (residues 421–456), was built manually by COOT in the experimental phasing map. The following density map was sharpened by solvent flattening using RESOLVE (54) and refined by phenix.refine (55). The twinned data with a one-twin law (k, h, -h-k-l) or triple twins (-h, -k, l/k, h, -l/-k, -h, -l) were detwinned by phenix.xtriage, and the rebuilt FIN219 model was refined by phenix.refine with the corresponding twin operators. The MR solution of the reconstructed FIN219 model achieved a better quality with superior log-likelihood-gain values, and we succeeded in finding the FIN219–FIP1 complex solution. The further improvement of map quality was obtained through twin-fraction refinement by REFMAC5 on the CCP4 platform (56). REFMAC5 filtered out those small twin fractions in the data and maintained the major twin domain with the target twin operator. The revised structure data were refined by phenix.refine, including generating new R-free flags. Ligand structures and geometry restraints were obtained using the eLBOW program on the PHENIX platform. Validation was performed by the MolProbity program for real-space correlation, molecular geometry, and Ramachandran plots. All structure models were prepared and demonstrated using PyMol.

FIN219 Adenylation Activity Assay. The kinetic assay for adenylation activities of FIN219, FIN219–FIP1, JAR1-1, and JAR1-3 involved the Taussky–Shorr method (40) for determining the production of inorganic phosphorus decomposed from pyrophosphate. Protein samples were incubated with 1×TBS, 5 mM $MgCl_2$, 2 mM DTT, 2 mM (±) jasmonic acid, 1 mM L-Ile, and various concentrations of ATP (0.1–5 mM) at 25 °C for 5 min and heated to 100 °C for 3 min. After cooling down to room temperature, 1 unit of pyrophosphatase was added to the sample, which was incubated at 25 °C for 5 min. After incubation, the Taussky–Shorr reagent was added to measure A_{650}. Taussky–Shorr reagent was prepared with 1 mM ammonium molybdate, 200 mM H_2SO_4, and 40 mM $FeSO_4{\cdot}7H_2O$ and stock at 4 °C. One unit of pyrophosphatase could almost catalyze 1 mM sodium pyrophosphatase to 2 mM inorganic phosphorus at 25 °C in 5 min and does not react with ATP.

FIP1 GST Activity Assay. The kinetic assay for GST activity of FIP1 was analyzed by the CDNB assay to determine the production of GS–DNB (28). Protein samples were incubated with 100 mM NaH_2PO_4 (pH 6.5), 1 mM GSH, and various concentrations of CDNB (0.1–3 mM) at 25 °C for 5 min. The produced GS-DNB was measured at A_{340}. The enzyme activity of SjGST expressed from pGEX-4T-1 vector was measured as a positive control, and FIN219 was measured as a negative control.

QCM Binding Assay. Molecular interaction of FIN219–FIP1 was analyzed by an AffinixQN quartz crystal microbalance biosensor (Initium, Inc.) (36). The converse piezoelectric effect is the basis of QCM sensing technology. It was reported in the 1950s that the frequency of a quartz crystal is proportional to the mass of the substance on an Au electrode. The relationship between change in frequency and the mass of an adherent substance is expressed by Sauerbrey's equation:

$$\Delta F = -\frac{2\Delta m n f_0^2}{A\mu_q^{1/2}\rho_q^{1/2}},$$

where ΔF is the measured frequency change, f_0 is the fundamental frequency of the quartz crystal before a mass change (27×10^6 Hz); Δm is the mass of the substance that adhered per electrode unit area; A is the electrode area; and ρ_q and μ_q, respectively, are the specific density and shear wave velocity in quartz. This formula shows that ΔF is proportional to mass Δm, and the 1-Hz vibration corresponds to 30 pg of mass change.

The principle of molecular interaction analysis by QCM is based on the Langmuir equation (also known as the Langmuir adsorption isotherm) (57), which depicts a relationship between the number of active sites of the surface undergoing adsorption and pressure. The equation is described as follows:

$$[\text{Host}] + [\text{Guest}] \underset{K_{off}}{\overset{K_{on}}{\rightleftharpoons}} [\text{Host}][\text{Guest}].$$

This reaction between the adsorbate surface (Host) and the adsorbate molecule (Guest) yields an adsorbed complex (Host–Guest). K_{on} ($M^{-1}{\cdot}min^{-1}$) and K_{off} (min^{-1}) are representative of the association and dissociation rate constants, respectively. According to the law of mass action, the ratio of K_{off} to K_{on} is the K_d (M) of receptor binding:

$$K_d = \frac{K_{off}}{K_{on}}.$$

Summing up the above equations, a formula is used to determine the relationship between adsorbed complex concentrations and frequency changes. It is described as below and according to the Langmuir equation:

$$\Delta F = \frac{B_{max}[\text{Guest}]}{K_d + [\text{Guest}]}.$$

B_{max} is representative of maximum frequency of molecular binding at equilibrium. The K_d and B_{max} values are calculated by nonlinear fitting based on the values of each point of monitored curves.

The biosensor was washed twice with 3 μL of piranha solution (H_2SO_4/H_2O_2 = 3:1) and incubated with 1% SDS for 5 min. Four hundred microliters of reaction buffer (20 mM Hepes, 0.2 M NaCl, 1 mM DTT, 1 mM EDTA) was applied to the dried sensor for balance and set up the magnetic stir at 1,000 rpm at 25 °C. FIP1 (1 mg/mL) was injected into buffer and coated on the Au electrode plate for saturation. Excess proteins were washed out with reaction buffer, and BSA (1 m/mL) was added to the buffer for sensor blocking until the oscillation frequency became a statically horizontal line. After blocking, the sensor was washed smoothly with reaction buffer and FIN219 (1 mg/mL) was injected into the buffer, waiting for frequency balance. The continuous titration method was used to determine the binding affinity of two molecules, and values were recorded as multiple binding curves by AFFINIXQN software. Data processing was performed by AQUA software from three independent experiments with the use of the equations given above.

Determination of Enzyme Kinetic Data Using a QCM Biosensor. The kinetic assay for enzyme activity was analyzed by an AffinixQN QCM biosensor, and similar experiments were described previously (58, 59). The kinetics equation, derived from the Langmuir adsorption model, is used to determine enzyme kinetics as follows:

$$\Delta Y = Y_{max}(1 - \exp(-K_{obs}) \times X),$$

$$K_{obs} = K_{off} + K_{on}[\text{Guest}],$$

where ΔY and Y_{max}, respectively, are the frequency variation in hertz and the maximum binding value in hertz; X is the experiment time; and K_{obs} (s^{-1}) is the observed rate constant. This Langmuir adsorption model is based on chemisorption, where molecules are able to adsorb to the surface and desorb reversibly. Both substrate–enzyme binding and release rate constants (K_{on} and K_{off}, respectively), as well as the adenylation rate constant (K_{cat}), can be obtained from time-dependent changes in frequency of the enzyme-immobilized QCM plate. The process of JA-Ile production catalyzed by FIN219 and FIN219–FIP1 is described by the Michaelis–Menten equation:

$$ES_{JA}S_{Ile} + S_{ATP} \underset{K_{off}}{\overset{K_{on}}{\rightleftharpoons}} ES_{JA}S_{Ile}S_{ATP} \overset{K_{cat}}{\rightarrow} EP_{JA\text{-}Ile} + P_{AMP} + P_{PPi},$$

where $ES_{JA}S_{Ile}S_{ATP}$ is the quaternary complex of FIN219–jasmonic acid–isoleucine–adenosine triphosphate, $P_{JA\text{-}Ile}$ is the product JA-Ile, and K_{cat} is the adenylation rate constant. The total masses of $ES_{JA}S_{Ile}S_{ATP}$ and $EP_{JA\text{-}Ile}$ are derived from the change in frequency after the binding process (shown in Fig. 4) in the bulk solution. When the initial velocities are plotted against ATP concentrations, saturation behavior is apparent (Fig. 4 *B* and *C*). The V_{max} ($nmol{\cdot}min^{-1}{\cdot}mg^{-1}$) value was determined according to the maximum change in frequency. The constants K_{on}, K_{off}, K_{obs}, and K_d are directly measured on the QCM. The K_{cat} for JA-Ile is obtained from the equation:

$$V_{max} = [E_t]K_{cat}.$$

The biosensor preparation and protein immobilization were performed as described above. All enzyme kinetics experiments include magnesium ion in reaction buffer for adenylation activity. Proteins were immobilized on the sensor plate for saturation and incubated with reaction buffer [20 mM Hepes, 0.2 M NaCl, 1 mM DTT, 1 mM (±) jasmonic acid, 1 mM L-Ile, 1 mM $MgCl_2$]. Various concentrations of ATP (0.1–1 mM) were injected independently into the sensor for catalysis reaction, and the frequency changes were recorded by AFFINIXQN software. Data processing was performed by AQUA software from three independent experiments with use of the equations given above.

ACKNOWLEDGMENTS. We thank the members of the H.-L.H. laboratory for discussion and assistance. We thank the Synchrotron Radiation Protein Crystallography Facility of the National Core Facility Program for Biotechnology, Ministry of Science and Technology and the National Synchrotron Radiation Research Center, a national user facility supported by the Ministry of Science and Technology, Taiwan, for technical services. This work is partly supported by Technology Commons, College of Life Science, National Taiwan University. Financial support was from the Taiwan Ministry of Science and Technology (Grant 104-2311-B-002-004 to Y.-S.C.) and National Taiwan University (Grants NTU-ICRP-104R7560-3 and NTU-CESRP-104R7614-2 to Y.-S.C.). This work is partly supported by Technology Commons, College of Life Science, National Taiwan University.

1. Hsieh HL, et al. (2000) FIN219, an auxin-regulated gene, defines a link between phytochrome A and the downstream regulator COP1 in light control of Arabidopsis development. *Genes Dev* 14(15):1958–1970.
2. Staswick PE, Tiryaki I, Rowe ML (2002) Jasmonate response locus JAR1 and several related Arabidopsis genes encode enzymes of the firefly luciferase superfamily that show activity on jasmonic, salicylic, and indole-3-acetic acids in an assay for adenylation. *Plant Cell* 14(6):1405–1415.
3. Hagen G, Kleinschmidt A, Guilfoyle T (1984) Auxin-regulated gene expression in intact soybean hypocotyl and excised hypocotyl sections. *Planta* 162(2):147–153.
4. Terol J, Domingo C, Talón M (2006) The GH3 family in plants: Genome wide analysis in rice and evolutionary history based on EST analysis. *Gene* 371(2):279–290.
5. Fu J, Yu H, Li X, Xiao J, Wang S (2011) Rice GH3 gene family: Regulators of growth and development. *Plant Signal Behav* 6(4):570–574.
6. Jain M, Kaur N, Tyagi AK, Khurana JP (2006) The auxin-responsive GH3 gene family in rice (Oryza sativa). *Funct Integr Genomics* 6(1):36–46.
7. Liao D, et al. (2015) The characterization of six auxin-induced tomato GH3 genes uncovers a member, SlGH3.4, strongly responsive to arbuscular mycorrhizal symbiosis. *Plant Cell Physiol* 56(4):674–687.
8. Kumar R, Agarwal P, Tyagi AK, Sharma AK (2012) Genome-wide investigation and expression analysis suggest diverse roles of auxin-responsive GH3 genes during development and response to different stimuli in tomato (Solanum lycopersicum). *Mol Genet Genomics* 287(3):221–235.
9. Feng S, et al. (2015) Genome-wide identification, expression analysis of auxin-responsive GH3 family genes in maize (Zea mays L.) under abiotic stresses. *J Integr Plant Biol* 57(9):783–795.
10. Schmelz S, Naismith JH (2009) Adenylate-forming enzymes. *Curr Opin Struct Biol* 19(6):666–671.
11. Chang KH, Xiang H, Dunaway-Mariano D (1997) Acyl-adenylate motif of the acyl-adenylate/thioester-forming enzyme superfamily: A site-directed mutagenesis study with the Pseudomonas sp. strain CBS3 4-chlorobenzoate:coenzyme A ligase. *Biochemistry* 36(50):15650–15659.
12. Okrent RA, Wildermuth MC (2011) Evolutionary history of the GH3 family of acyl adenylases in rosids. *Plant Mol Biol* 76(6):489–505.
13. Chini A, et al. (2007) The JAZ family of repressors is the missing link in jasmonate signalling. *Nature* 448(7154):666–671.
14. Wang JG, Chen CH, Chien CT, Hsieh HL (2011) FAR-RED INSENSITIVE219 modulates CONSTITUTIVE PHOTOMORPHOGENIC1 activity via physical interaction to regulate hypocotyl elongation in Arabidopsis. *Plant Physiol* 156(2):631–646.
15. Guranowski A, Miersch O, Staswick PE, Suza W, Wasternack C (2007) Substrate specificity and products of side-reactions catalyzed by jasmonate:amino acid synthetase (JAR1). *FEBS Lett* 581(5):815–820.
16. Staswick PE, Tiryaki I (2004) The oxylipin signal jasmonic acid is activated by an enzyme that conjugates it to isoleucine in Arabidopsis. *Plant Cell* 16(8):2117–2127.
17. Doares SH, Syrovets T, Weiler EW, Ryan CA (1995) Oligogalacturonides and chitosan activate plant defensive genes through the octadecanoid pathway. *Proc Natl Acad Sci USA* 92(10):4095–4098.
18. Svoboda J, Boland W (2010) Plant defense elicitors: Analogues of jasmonoyl-isoleucine conjugate. *Phytochemistry* 71(13):1445–1449.
19. Turner JG, Ellis C, Devoto A (2002) The jasmonate signal pathway. *Plant Cell* 14(Suppl): S153–S164.
20. Wasternack C, Forner S, Strnad M, Hause B (2013) Jasmonates in flower and seed development. *Biochimie* 95(1):79–85.
21. Balbi V, Devoto A (2008) Jasmonate signalling network in Arabidopsis thaliana: Crucial regulatory nodes and new physiological scenarios. *New Phytol* 177(2):301–318.
22. Koo AJ, Gao X, Jones AD, Howe GA (2009) A rapid wound signal activates the systemic synthesis of bioactive jasmonates in Arabidopsis. *Plant J* 59(6):974–986.
23. Glauser G, et al. (2008) Spatial and temporal dynamics of jasmonate synthesis and accumulation in Arabidopsis in response to wounding. *J Biol Chem* 283(24): 16400–16407.
24. Browse J, Howe GA (2008) New weapons and a rapid response against insect attack. *Plant Physiol* 146(3):832–838.
25. Ballaré CL (2014) Light regulation of plant defense. *Annu Rev Plant Biol* 65:335–363.
26. Robson F, et al. (2010) Jasmonate and phytochrome A signaling in Arabidopsis wound and shade responses are integrated through JAZ1 stability. *Plant Cell* 22(4):1143–1160.
27. Edwards R, Dixon DP (2005) Plant glutathione transferases. *Methods Enzymol* 401:169–186.
28. Dixon DP, Edwards R (2010) Glutathione transferases. *Arabidopsis Book* 8:e0131.
29. Axarli I, Dhavala P, Papageorgiou AC, Labrou NE (2009) Crystal structure of Glycine max glutathione transferase in complex with glutathione: Investigation of the mechanism operating by the Tau class glutathione transferases. *Biochem J* 422(2):247–256.
30. Chen IC, et al. (2007) Glutathione S-transferase interacting with far-red insensitive 219 is involved in phytochrome A-mediated signaling in Arabidopsis. *Plant Physiol* 143(3): 1189–1202.
31. Wagner U, Edwards R, Dixon DP, Mauch F (2002) Probing the diversity of the Arabidopsis glutathione S-transferase gene family. *Plant Mol Biol* 49(5):515–532.
32. Dixon DP, Skipsey M, Edwards R (2010) Roles for glutathione transferases in plant secondary metabolism. *Phytochemistry* 71(4):338–350.
33. Westfall CS, et al. (2012) Structural basis for prereceptor modulation of plant hormones by GH3 proteins. *Science* 336(6089):1708–1711.
34. Round A, et al. (2013) Determination of the GH3.12 protein conformation through HPLC-integrated SAXS measurements combined with X-ray crystallography. *Acta Crystallogr D Biol Crystallogr* 69(Pt 10):2072–2080.
35. Westfall CS, Muehler AM, Jez JM (2013) Enzyme action in the regulation of plant hormone responses. *J Biol Chem* 288(27):19304–19311.
36. Marx KA (2003) Quartz crystal microbalance: A useful tool for studying thin polymer films and complex biomolecular systems at the solution-surface interface. *Biomacromolecules* 4(5):1099–1120.
37. Poornam GP, Matsumoto A, Ishida H, Hayward S (2009) A method for the analysis of domain movements in large biomolecular complexes. *Proteins* 76(1):201–212.
38. Thom R, et al. (2002) Structure of a tau class glutathione S-transferase from wheat active in herbicide detoxification. *Biochemistry* 41(22):7008–7020.
39. Peat TS, et al. (2012) Crystal structure of an indole-3-acetic acid amido synthetase from grapevine involved in auxin homeostasis. *Plant Cell* 24(11):4525–4538.
40. Taussky HH, Shorr E (1953) A microcolorimetric method for the determination of inorganic phosphorus. *J Biol Chem* 202(2):675–685.
41. Suza WP, Staswick PE (2008) The role of JAR1 in Jasmonoyl-L: -Isoleucine production during Arabidopsis wound response. *Planta* 227(6):1221–1232.
42. Gulick AM (2009) Conformational dynamics in the Acyl-CoA synthetases, adenylation domains of non-ribosomal peptide synthetases, and firefly luciferase. *ACS Chem Biol* 4(10):811–827.
43. Kazan K, Manners JM (2011) The interplay between light and jasmonate signalling during defence and development. *J Exp Bot* 62(12):4087–4100.
44. Conti E, Franks NP, Brick P (1996) Crystal structure of firefly luciferase throws light on a superfamily of adenylate-forming enzymes. *Structure* 4(3):287–298.
45. Cardoso RM, Daniels DS, Bruns CM, Tainer JA (2003) Characterization of the electrophile binding site and substrate binding mode of the 26-kDa glutathione S-transferase from Schistosoma japonicum. *Proteins* 51(1):137–146.
46. Rossel JB, Wilson IW, Pogson BJ (2002) Global changes in gene expression in response to high light in Arabidopsis. *Plant Physiol* 130(3):1109–1120.
47. Dixon DP, Edwards R (2009) Selective binding of glutathione conjugates of fatty acid derivatives by plant glutathione transferases. *J Biol Chem* 284(32):21249–21256.
48. Mishra R, Seckler R, Bhat R (2005) Efficient refolding of aggregation-prone citrate synthase by polyol osmolytes: How well are protein folding and stability aspects coupled? *J Biol Chem* 280(16):15553–15560.
49. McPhillips TM, et al. (2002) Blu-Ice and the Distributed Control System: Software for data acquisition and instrument control at macromolecular crystallography beamlines. *J Synchrotron Radiat* 9(Pt 6):401–406.
50. Otwinowski Z, Minor W (1997) Processing of X-ray diffraction data collected in oscillation mode. *Methods Enzymol* 276:307–326.
51. Adams PD, et al. (2010) PHENIX: A comprehensive Python-based system for macromolecular structure solution. *Acta Crystallogr D Biol Crystallogr* 66(Pt 2):213–221.
52. MacRae IJ, Doudna JA (2007) An unusual case of pseudo-merohedral twinning in orthorhombic crystals of Dicer. *Acta Crystallogr D Biol Crystallogr* 63(Pt 9):993–999.
53. McCoy AJ, et al. (2007) Phaser crystallographic software. *J Appl Cryst* 40(Pt 4):658–674.
54. Terwilliger TC (2001) Maximum-likelihood density modification using pattern recognition of structural motifs. *Acta Crystallogr D Biol Crystallogr* 57(Pt 12):1755–1762.
55. Afonine PV, et al. (2012) Towards automated crystallographic structure refinement with phenix.refine. *Acta Crystallogr D Biol Crystallogr* 68(Pt 4):352–367.
56. Winn MD, et al. (2011) Overview of the CCP4 suite and current developments. *Acta Crystallogr D Biol Crystallogr* 67(Pt 4):235–242.
57. Langmuir I (1918) The adsorption of gases on plane surfaces of glass, mica and platinum. *J Am Chem Soc* 40:1361–1403.
58. Nihira T, Mori T, Asakura M, Okahata Y (2011) Kinetic studies of dextransucrase enzyme reactions on a substrate- or enzyme-immobilized 27 MHz quartz crystal microbalance. *Langmuir* 27(6):2107–2111.
59. Souto DEP, Faria AR, de Andrade HM, Kubota LT (2015) Using QCM and SPR for the kinetic evaluation of the binding between a new recombinant chimeric protein and specific antibodies of the visceral leishmaniasis. *Curr Protein Pept Sci* 16(8):782–790.